

# Journal of Materials Chemistry A

Accepted Manuscript



This is an *Accepted Manuscript*, which has been through the Royal Society of Chemistry peer review process and has been accepted for publication.

*Accepted Manuscripts* are published online shortly after acceptance, before technical editing, formatting and proof reading. Using this free service, authors can make their results available to the community, in citable form, before we publish the edited article. We will replace this *Accepted Manuscript* with the edited and formatted *Advance Article* as soon as it is available.

You can find more information about *Accepted Manuscripts* in the [Information for Authors](#).

Please note that technical editing may introduce minor changes to the text and/or graphics, which may alter content. The journal's standard [Terms & Conditions](#) and the [Ethical guidelines](#) still apply. In no event shall the Royal Society of Chemistry be held responsible for any errors or omissions in this *Accepted Manuscript* or any consequences arising from the use of any information it contains.

Cite this: DOI: 10.1039/c0xx00000x

www.rsc.org/xxxxxx

ARTICLE TYPE

# Approaching the top of the emissive properties of CH<sub>3</sub>NH<sub>3</sub>PbBr<sub>3</sub> perovskite nanoparticles

Soranyel Gonzalez-Carrero,<sup>a</sup> Raquel E. Galian\*<sup>a</sup> and Julia Pérez-Prieto\*<sup>a</sup>

Received (in XXX, XXX) Xth XXXXXXXXXX 20XX, Accepted Xth XXXXXXXXXX 20XX

DOI: 10.1039/b000000x

Highly luminescent and photostable CH<sub>3</sub>NH<sub>3</sub>PbBr<sub>3</sub> nanoparticles have been prepared by fine-tuning the molar ratio between CH<sub>3</sub>NH<sub>3</sub>Br, PbBr<sub>2</sub>, a medium-size alkyl-chain ammonium salt, and 1-octadecene. They exhibit a unique photoluminescence quantum yield (ca. 83%) and average recombination lifetime (ca. 600 ns) in toluene dispersion.

## 1. Introduction

Currently there is a great interest in organolead halide perovskites with the general formula of APbX<sub>3</sub> (A= organic ammonium cation, X = halide anion). They present a three-dimensional (3D) inorganic framework consisting of corner-sharing PbX<sub>6</sub> octahedra and small-sized organic cations in the voids between the octahedra.

Organometal halide perovskites combine the favourable properties of the inorganic semiconductor, namely its great charge carrier mobility, with the flexibility and low-temperature processability of the organic material.<sup>1</sup> In particular, methylammonium (MA) lead trihalide perovskite materials allow low-cost solution processing, and they absorb broadly across the solar spectrum. Easy and fast generation of the charge carriers, transport of both electrons and holes, and high photoluminescence (PL) efficiency are desirable properties for optoelectronic devices.<sup>2-5</sup>

The revolution in the use of hybrid perovskites as novel materials for solid state solar cells started in 2012, when Grätzel and Snaith reported, practically at the same time, photovoltaic power conversion efficiencies of 9.7% and 10.9%, respectively.<sup>6-8</sup> In this regard, thin films of organometal halide perovskites have been recently prepared by vapour deposition, but the functional perovskites have mostly been prepared as nanoparticulate material by using a template method, specifically by making use of the pores of mesoporous TiO<sub>2</sub> and Al<sub>2</sub>O<sub>3</sub>,<sup>9</sup> which in the case of TiO<sub>2</sub> it also acts as an electron transporter. It is likely that these mesoporous materials also improve the uniformity of the perovskite coating.

Remarkably, thin films of MAPbI<sub>3-x</sub>Cl<sub>x</sub> mixed halide perovskites capped by poly(methyl methacrylate), PMMA, have shown a high charge mobility and low bimolecular nonradiative recombination (PL decay of ca. 273 ns), thus making it possible to generate carrier diffusion lengths that exceed 1 micron; comparatively, PL decay of MAPbI<sub>3</sub> was ca. 96.6 ns and the

carrier diffusion length was ca. 100 nm.<sup>10</sup>

Recently, studies on the photophysical properties of simply solution-processed crystalline films of these organic-metallic mixed halides, prepared by spin coating followed by annealing at 100 °C and subsequently capped with a thin layer of PMMA, showed that, at room temperature, they exhibited moderate to high PL quantum efficiency depending on the excitation density (from 35% at 25 μJ/cm<sup>2</sup> to 70% at 1 mJ/cm<sup>2</sup>).<sup>4</sup> The decreased PL efficiency at low excitation densities was attributed to the presence of defects that caused nonradiative decay, and it was suggested that at high excitation density the defects were filled and radiative recombination became dominant. Photoexcitation in the pristine perovskite caused the formation of free charge carriers within 1 picosecond; the carriers underwent bimolecular recombination on the time scale of tens of nanoseconds at the higher excitation densities. The long carrier lifetimes together with the exceptionally high luminescence yield of the films were unique in these simply prepared inorganic semiconductors. The high PL efficiency evidenced the small contribution of nonradiative pathways to the PL decay of these materials and this is highly relevant and contrasts with the relatively low emission of other semiconductors when they are not capped with a high energy gap inorganic shell (as the CdSe nanoparticles).<sup>11</sup>

The improved performance of the MAPbI<sub>3-x</sub>Cl<sub>x</sub> mixed halide perovskite compared with that of MAPbI<sub>3</sub> in meso-structured solar cells has been attributed to lower charge recombination rates rather than to better charge mobility.<sup>12</sup>

A critical issue of organolead iodide perovskite materials is their stability. MAPbI<sub>3</sub> perovskite reverts to its precursors; this is attributed to the hygroscopic amine salts.<sup>13</sup> However the bromide-based perovskites have proved to be less moisture-sensitive.<sup>14</sup>

Bromide MAPbBr<sub>3</sub> perovskite can be applied as a light absorber for high energy photons and they can serve as the front cell in tandem cells. This perovskite can provide a higher open-circuit voltage in perovskite solar cells than the iodide analogue.<sup>15-16</sup>

However, the optical performance of MAPbBr<sub>3</sub> perovskite is

considerably lower than that of the mixed Br/Cl perovskites.

Thin films of MAPbBr<sub>3-x</sub>Cl<sub>x</sub> perovskites have been prepared by spin-coating of mixtures of the perovskite precursors on top of an Al<sub>2</sub>O<sub>3</sub> mesoporous layer, followed by heating at 100 °C.

Particularly, MAPbBr<sub>2.4</sub>Cl<sub>0.6</sub> (λ<sub>max</sub> at 525 nm, average recombination lifetime, τ<sub>av</sub>, 446 ns) exhibited the strongest PL emission of the mixed bromide/chloride perovskites. The τ<sub>av</sub> of CH<sub>3</sub>NH<sub>3</sub>PbBr<sub>3-x</sub>Cl<sub>x</sub> perovskites was much longer than that of MAPbI<sub>3-x</sub>Cl<sub>x</sub>; this suggested better charge diffusion properties of the former compounds. Under the same conditions, MAPbBr<sub>3</sub> perovskite showed much shorter lifetime (τ<sub>av</sub> of 100 ns; λ<sub>max</sub> at 530 nm).<sup>14</sup>

We have recently reported that six-nm sized MAPbBr<sub>3</sub> perovskite nanoparticles can exhibit a considerable PL quantum yield (ca. 20% as colloidal solution and film; λ<sub>max</sub> at 530 nm) at low excitation densities.<sup>17</sup> They were prepared by simply confining the 3D inorganic framework with octylammonium bromide (OABr). The method consisted of using a 1:1 molar ratio between the total ammonium salt and PbBr<sub>2</sub> concentration, an OABr/MABr molar ratio of 0.6:0.4, in the presence of oleic acid (OLA), and 1-octadecene (ODE). The role of the latter two in the emissive properties of the nanoparticles, if any, was not studied. Electroluminescent measurements of the film prepared from the colloidal solution exhibited ten times more response than that from the bulk material.

Encouraged by our preliminary results and those mentioned above, we then focused on performing a better organic capping of the bromide nanoparticles taking into account that surface states would be highly accessible to passivation treatment.<sup>18-19</sup> We envisaged that some methyl ammonium salt could be lost during the nanoparticle preparation and that MABr/PbBr<sub>2</sub> molar ratios greater than one could be advantageous.

We report here the preparation of highly dispersible MAPbBr<sub>3</sub> nanoparticles (Figure 1), which exhibit an extraordinarily high photoluminescence quantum yield and lifetime, in both toluene solution and film, as well as a high stability and photostability. They have been prepared by a non-template strategy adjusting the molar ratio between the total ammonium salts and PbBr<sub>2</sub>, the OABr/MABr/ODE molar ratio, and not using oleic acid.



**Fig. 1:** Picture of toluene dispersion of CH<sub>3</sub>NH<sub>3</sub>PbBr<sub>3</sub> nanoparticles under (a) the lab light and (b) UV-laser pointer excitation.

## 2. Experimental Section

### 2.1 Materials and methods

All chemicals were analytical grade and used as received without further purifications. Toluene was of HPLC quality for spectroscopic measurements.

#### UV-visible measurements

UV-vis spectra were recorded at room temperature using a quartz cuvettes spectrometer in a UV-visible spectrophotometer Agilent 8453E.

#### Photoluminescence steady state studies

Steady-state photoluminescence spectra (LPS-220B, motor driver (MD-5020), Brytebox PTI) were measured at room temperature on a spectrofluorometer PTI equipped with a lamp power supply. The Felix 32 Analysis software was used to register the data. All the data were acquired using 1cm×1cm path length quartz cuvettes.

The emission spectra (λ<sub>exc</sub> = 350 nm) of the perovskites dispersed in toluene were measured under air atmosphere (unless otherwise indicated).

The photoluminescence spectra and quantum yields of the films were measured with a Hamamatsu C9920-02 absolute PL Quantum Yield Measurement System (λ<sub>exc</sub> = 350 nm).

#### Time resolved photoluminescence

Experiments were done using a Compact fluorescence lifetime spectrometer C11367, Quantaurus-Tau with a LED pulse light source of 340, 405, and 470 nm. The average lifetime was obtained from the tri-exponential decays.

#### Microscopy images

Structural and morphological characterization were performed using bright field transmission electron microscopy (TEM), dark field TEM, selected area electron diffraction (SAED) and high resolution TEM (HRTEM). All these characterization techniques were carried out by using a Field Emission Gun (FEG) TECNAI G2 F20 microscope, operated at 200 kV. TEM samples were prepared by depositing a few drops of the perovskite solution on carbon film supported on a copper grid (200 mesh); they were subsequently dried overnight.

#### X-Ray Power Diffraction (XRPD)

The XRD analysis were performed in a powder diffractometer D8 Avance A25 model Bruker, with a powder diffractometer θ-θ configuration, X-ray tubes on a lineal receiver Cu radiation, and plus DIFFRAC EVA Data assessment program.

#### Nuclear magnetic resonance (<sup>1</sup>H-NMR)

The spectra were registered at room temperature in a Bruker DPX300 spectrometer, with a 300 MHz Bruker magnet (7 T). The chemical shifts (δ) are informed in ppm relative to tetramethylsilane (TMS).

#### Thermogravimetry analysis (TGA)

The TGA was carried out using a Mettler Toledo TGA/SDTA 851e system with an operative temperature range 25-1100°C and 0.1 microgram sensitivity. The samples were heated from 25 to 800 °C, with a increase of 10°C /min and under nitrogen flux of 40 mL/min.

#### X-Ray photoelectron spectroscopy (XPS)

The XPS data were acquired with Specs using a Phoibos 150-9MCD X-ray photoelectron spectrometer. The incident radiation was 50 W. The C 1s peak at 285 eV was set as a reference for all XPS peak positions.

### 2.2 Synthesis of nanoparticles

#### Synthesis of P<sub>OAI</sub>

A solution of oleic acid (OLA, 0.30 mmol, 85 mg) in 1-octadecene (ODE, 6.26 mmol, 2.0 mL) was stirred and heated at 80°C and then octylammonium bromide (OABr, 0.16 mmol, 33.5 mg) was added. Subsequently, methylammonium bromide (MABr, 0.24 mmol, 26.4 mg, dissolved in 100 μL of DMF) and

lead (II) bromide (0.10 mmol, 36.7 mg, dissolved in 200  $\mu\text{L}$  of DMF) were added. No color change was observed after the addition of lead (II) bromide. The solution was cooled down to 60  $^{\circ}\text{C}$  and immediately after the addition of acetone (5 mL) induced the precipitation of a yellow precipitate. The unreactive material was separated by centrifugation (7000 rpm, 10 min, 20 $^{\circ}\text{C}$ ).

Samples  $\text{P}_{\text{OA}2}$  and  $\text{P}_{\text{OA}3}$  were prepared following the same procedure but in the absence of OLA and ODE, respectively (see Table S1 for details).

### 10 Film preparation

Quartz substrates were extensively cleaned using detergent, de-mineralized water, and isopropyl alcohol, respectively, followed by 20 min UV-ozone treatment cleaning in order to enhance good thin film formation. A solution of perovskite in 15 toluene was spin-coated on top of the quartz substrates with 1500 rpm during 60s resulting in the film formation.

### Photostability assays

The photostability of the samples  $\text{P}_{\text{OA}1}$  and  $\text{P}_{\text{OA}2}$  was analysed using two different irradiation sources. Thus, toluene colloidal 20 solutions in 10x10 mm quartz cuvettes were irradiated in a Luzchem photoreactor equipped with eight visible lamps (380-490 nm, maximum at 419 nm with a dose 70.02  $\text{Wm}^{-2}$  in the 401-700 nm range). The room temperature photoluminescence of the samples ( $\lambda_{\text{exc}} = 350$  nm,  $\lambda_{\text{em}} = 521$  nm) was recorded every 5 min.

In addition, 10x10 mm quartz cuvettes containing the colloidal 25 solutions were placed in the sample-holder of a PTI- LPS-220B spectrometer equipped with a Xenon lamp (75 W) and the samples were illuminated with UV-light ( $\lambda_{\text{exc}} = 350$  nm). The Felix 32 analysis software was used to register the data.

## 30 3. Results and Discussion

### 3.1 Synthesis of $\text{CH}_3\text{NH}_3\text{PbBr}_3$ nanoparticles

The preparation of the nanoparticles was assayed by following our previously reported non-template strategy<sup>17</sup>, but using a 35 larger molar ratio between the total ammonium (OABr plus MABr) and  $\text{PbBr}_2$  salts (specifically 4:1) and varying the relative molar ratio between the ammonium salts (from 0.8:3.2 to 2.4:1.6). The amount of oleic acid (OLA) was maintained (3:1 OLA/ $\text{PbBr}_2$  molar ratio), while the ODE/ $\text{PbBr}_2$  molar ratio was fixed at 62.6:1.0. A control sample ( $\text{P}_c$ ) lacking the OABr was also prepared under the same reaction conditions and quantities of all the other compounds. As expected the solid  $\text{P}_c$  obtained after precipitation/centrifugation from the control experiment was hardly dispersible in toluene and it exhibited an emission 45 maximum at  $\lambda_{\text{max}} = 538$  nm, i.e., at a wavelength close to that of the bulk  $\text{MAPbBr}_3$  perovskite. By contrast, we obtained a more dispersible and emissive perovskite ( $\text{P}_{\text{OA}1}$ ) when adding OABr and using an OA/MA/ $\text{PbBr}_2$  molar ratio of 1.6:2.4:1. The change of the OA/MA/ $\text{PbBr}_2$  molar ratio to 2.4:1.6:1 led to a colloid 50 solution whose emission spectrum showed several peaks, which evidenced the formation of a mixture of perovskites with different stoichiometry (spectrum not shown).

Figure S1 in the supporting information shows the comparison between the absorption and emission ( $\lambda_{\text{ex}} = 350$  nm) spectra of the toluene dispersion of  $\text{P}_c$  sample and that of  $\text{P}_{\text{OA}1}$ . Toluene dispersion of  $\text{P}_{\text{OA}1}$  exhibited a peak emission considerably blue-shifted compared with that of  $\text{P}_c$  (513 nm vs 538 nm). In addition,

the emission spectrum of the film prepared from the toluene dispersion of  $\text{P}_{\text{OA}1}$  exhibited a red-shifted peak at  $\lambda_{\text{max}} = 526$  nm, 60 a slightly broader peak (full width at the half maximum, fwhm, 36 nm vs 31 nm), and a smaller emission quantum yield (34% vs 67%) than that of the toluene dispersion.

Then we evaluated the role of OLA on the optical properties of the nanoparticles. The preparation of the nanoparticles was carried out under the same reaction conditions, using the OA/MA/ $\text{PbBr}_2$  molar ratio of 1.6:2.4:1 and maintaining the amount of ODE but in the absence of OLA (Table S1). After precipitation and centrifugation the solid  $\text{P}_{\text{OA}2}$  was dispersed in toluene.

70 Interestingly, there was an improvement in the optical properties of both the colloidal perovskite solution and the film prepared from it (Figure 2). Thus, i) the absorption spectrum of the colloidal solution showed less scattering than when the nanoparticles were prepared in the presence of OLA, ii) they exhibited an enhanced emission (ca. 83% yield for the colloid and 72% for the film), and iii) the emission band of the film was even narrower (fwhm of 30 nm vs 32 nm for the colloidal dispersion).

The role of ODE on the eventual optical performance of the nanoparticles was also analysed by conducting the nanoparticle 80 preparation in the same reaction conditions to that of sample  $\text{P}_{\text{OA}1}$  (OA/MA/ $\text{PbBr}_2$  molar ratio of 1.6:2.4:1, oleic acid/ $\text{PbBr}_2$  molar ratio of 3:1), but in the absence of ODE (Table S1). This sample ( $\text{P}_{\text{OA}3}$ ) exhibited an emission quantum yield ca. 52% yield in toluene dispersion and ca. 41% in the film (see spectra in Figure 85 S2).

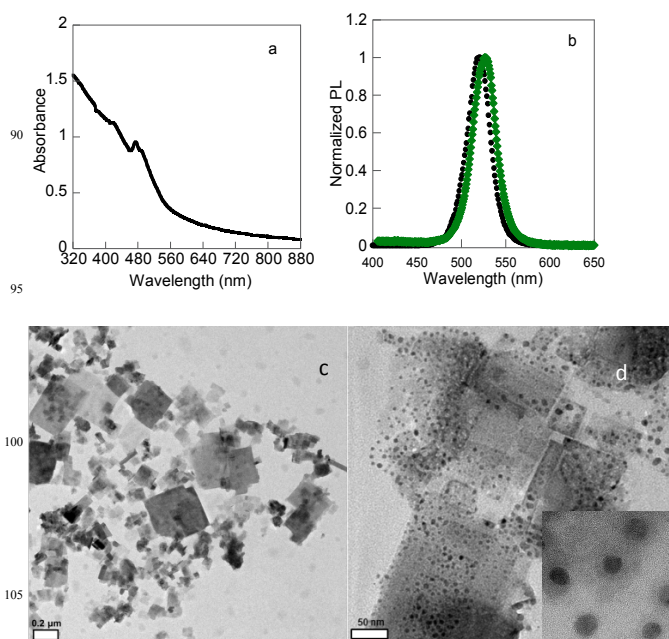


Fig. 2. (a) Absorption spectrum of  $\text{P}_{\text{OA}2}$  in toluene solution and (b) normalized emission ( $\lambda_{\text{exc}} = 350$  nm) spectra of  $\text{P}_{\text{OA}2}$  in toluene solution (●) and film (◆); (c and d) HRTEM images of  $\text{P}_{\text{OA}2}$ ; scale bar of 0.2  $\mu\text{m}$  (c) and 50 nm (d); inset: HRTEM image of  $\text{P}_{\text{OA}2}$ , scale bar of 5 nm.

The influence of the alkyl-chain length of the longer ammonium salt on the emissive properties of the nanomaterial was also analysed (Table S2). The reaction was carried out using 115 ethylammonium bromide (EABr), hexylammonium bromide

(HABr), and octadecylammonium bromide (ODABr), instead of OABr, and under all the same conditions as that used for the preparation of  $P_{OA2}$ . A non-dispersible perovskite was obtained in the case of EABr, while ODABr led to a perovskite with a lower-dimension framework (spectra not shown). However, HABr led to a perovskite ( $P_{HXA}$ ) dispersible in toluene and exhibiting a narrow emission at  $\lambda_{max}$  526 nm, i.e., 5 nm red-shifted compared to that of  $P_{OA2}$  (Figure S3). The PL quantum yield was lower than that of  $P_{OA1}$  and  $P_{OA2}$  (specifically, 58% for the colloidal dispersion and 38% for the film).

Regarding the size of the particles, high resolution transmission electron microscopy (HRTEM) analyses of the emissive samples showed that smaller nanoparticles were obtained in the absence of OLA and ODE. Thus,  $P_{OA2}$  and  $P_{OA3}$  consisted of spherical nanoparticles with an average size of  $5.5 \pm 1.5$  nm and  $5.9 \pm 1.8$  nm, respectively (see Figure 2 for  $P_{OA2}$  and Figure S2 for  $P_{OA3}$ ), while  $P_{OA1}$  comprised spherical nanoparticles with an average size of  $7.0 \pm 1.5$  nm. In all the cases, most of the nanoparticles were embedded in an amorphous material forming plaques, which were smaller in the case of  $P_{OA2}$  (most of them  $60 \text{ nm} \times 50 \text{ nm}$ ).

The fast Fourier transform (FFT) patterns of  $P_{OA1}$  and  $P_{OA2}$  nanoparticles showed that they possessed crystalline surfaces. The lattice spacing in the HRTEM image and FFT patterns were in agreement with the crystallographic parameters for the  $\text{CH}_3\text{NH}_3\text{PbBr}_3$  bulk material. The interplanar spacing determined from the FFT patterns were of 5.91, 4.11, 3.48 and 2.94 Å, which can be attributed to the 001, 011, 111 and 002 family planes of cubic phase structure of  $\text{CH}_3\text{NH}_3\text{PbBr}_3$  with Pm-3m space group. In addition, the X-ray powder diffraction (XRPD) analysis of the solid  $P_{OA1}$  and  $P_{OA2}$  confirmed the phase purity of the perovskites as well as the crystallinity of the samples (Figure 3).

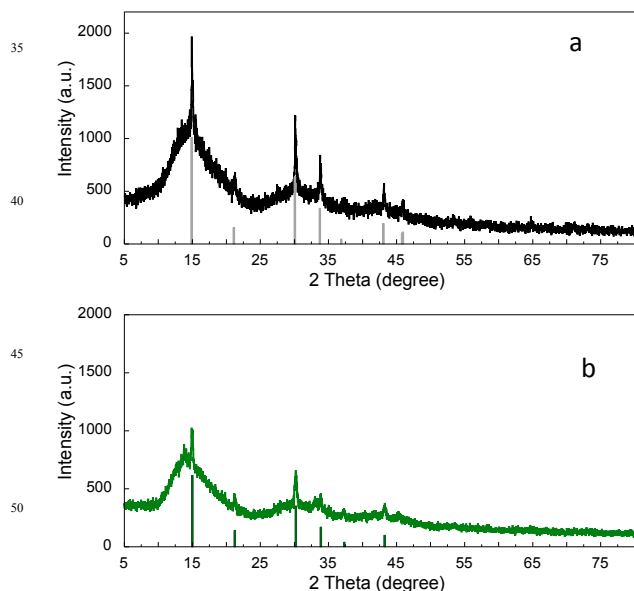


**Fig. 3:** X-ray diffraction pattern of  $P_{OA1}$  (a) and  $P_{OA2}$  (b). The vertical bars correspond to the peaks of  $\text{CH}_3\text{NH}_3\text{PbBr}_3$  cubic phase.

The XRPD pattern of the samples demonstrated that they presented an excellent fit to a single-phase model corresponding

to the cubic phase of the hybrid organic-inorganic  $\text{MAPbBr}_3$  perovskite ( $a = 5.9334$  (5) Å, space group = Pm3m).<sup>20-21</sup> The XRPD peaks of the samples were very broad. This is consistent with the formation of  $\text{MAPbBr}_3$  mostly as nanoparticles, particularly in the case of  $P_{OA2}$ .

The X-ray photoelectron microscopy (XPS) spectra of  $P_{OA1}$  and  $P_{OA2}$  were analysed, using a C peak at 285.0 eV as reference. Remarkably, in general, all the peaks of  $P_{OA2}$  were slightly shifted to a higher binding energy compared to those of  $P_{OA1}$  (see Fig S4-S8). In both samples, the XPS spectrum of Pb 4f showed two symmetric peaks attributed to Pb 4f<sub>7/2</sub> and Pb 4f<sub>5/2</sub> level at binding energies (BE) of ca. 138.7 eV and 143.6, respectively. The spin orbit split between the Pb 4f<sub>7/2</sub> and Pb 4f<sub>5/2</sub> levels was of 4.9 eV which agrees with the value reported in the literature (4.8 eV)<sup>22</sup> very small peak at lower binding energy (ca. 136.8 eV) could be attributed to the presence of metallic lead and it has also been detected in the XPS spectra of  $\text{CH}_3\text{NH}_3\text{PbI}_3/\text{TiO}_2$  system.<sup>23</sup>

The Br 3d XPS BE of the perovskite was at ca. 69.1 eV. The N1s XPS spectra showed the presence of one peak at 402.6 eV corresponding to the -N- of the ammonium salts.<sup>24</sup> In addition, a very small peak at ca. 400.0 eV was also detected in the case of  $P_{OA1}$ ; this could be assigned to a small amount of free amines.<sup>25</sup>

The deconvolution of the C1s XPS spectra gave two peaks at ca. 285.7 and 285.0 eV. While that at the lower energy value can be attributed to C-C/ C-H bond, plus to the C=C bond of OLA and ODE, the peak at 285.7 eV, could be assigned to the C-N<sup>+</sup> bond of the ammonium salts.<sup>26</sup> The spectra showed the larger contribution of the peak at BE of ca. 285.7 eV for  $P_{OA2}$  than for  $P_{OA1}$ ; this is consistent with that found in the analysis of the composition of the nanoparticles by <sup>1</sup>H-NMR and TGA (see below).

Finally, the O1s XPS band at 532.9 eV was accompanied in the case of  $P_{OA1}$  by a small band at 528.8 eV that was consistent with the presence of small amounts of PbO.<sup>27</sup> The formation of the PbO could be tentatively attributed to the presence of oleic acid in the preparation of the nanoparticles.<sup>28</sup>

Quantification of lead and bromine by XPS led to a 73:28 molar ratio for  $P_{OA2}$  while it was 68:32 for  $P_{OA1}$ .

### 3.2 Analysis of the composition of the $\text{CH}_3\text{NH}_3\text{PbBr}_3$ nanoparticle samples

The composition of  $P_{OA1}$  and  $P_{OA2}$ , obtained after their precipitation/centrifugation step, as well as the composition of the resulting supernatant, were studied by using thermogravimetric analysis (TGA) and <sup>1</sup>H-NMR. Solvent removal from the supernatant followed by addition of ethyl ether caused the precipitation of a solid (Ss). In addition, the ether solution was distilled, thus recovering ODE accompanied by OABr (plus OLA in the case of the synthesis of  $P_{OA1}$ ).

The TGA of  $P_{OA1}$  and  $P_{OA2}$  samples was compared with that of the individual precursors (MABr, OABr, ODE, OLA, lead bromide), as well as with that of methylamine and octylamine (see TGA of all the precursors in Figures S9-S11). The peak of the first derivative indicates the point of greatest rate of change on the weight loss curve. TGA of  $P_{OA1}$  (Figure 4) showed it lost ca. 16.0% of its weight before reaching ~200 °C, followed by a weight loss of ca. 24.0% before reaching ~360 °C (corresponding to at least two different components), and then a weight loss of 56.6% before reaching 600 °C. The spectrum

showed that 2.6% of the mass that did not decompose or sublime at temperatures of up to 800 °C. The remaining residue may be impurities present in the material or decomposition products. The peaks of the first derivative were at 178, 345, and 580 °C.

The trend in sample **P<sub>OA2</sub>** (Figure 4) was quite similar but the temperature of the first derivative peaks shifted to higher values (183, 358, and 616 °C), suggesting a higher stability of the components that build the nanoparticle in the absence of oleic acid. Sample **P<sub>OA2</sub>** lost 17.63% weight before reaching ~210 °C, followed by a weight loss of ca. 24.15% before reaching ~380 °C (corresponding to at least two different components), and then a weight loss of 58.05% before reaching the 650 °C. In addition, it did completely sublime at temperatures below 700 °C.

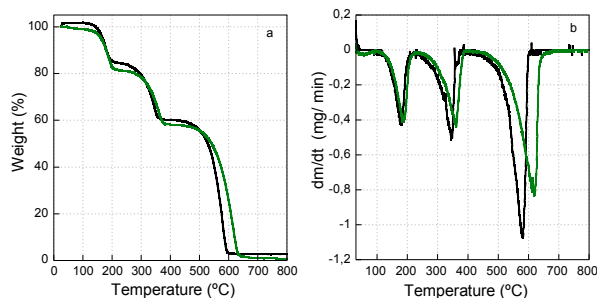


**Fig. 4:** TGA heating curves of **P<sub>OA1</sub>** (black) and **P<sub>OA2</sub>** (green) nanoparticle expressed as weight % as a function of applied temperature (a) and the corresponding 1<sup>st</sup> derivatives (b).

The first loss of weight in sample **P<sub>OA1</sub>** and sample **P<sub>OA2</sub>** could be attributed to a loss of octylamine, but there was no matching between the temperatures of the first derivative peaks of these peaks and that of the amines (Figure S11). In addition, MABr and OABr ammonium salts underwent weight loss at a temperature of over 200 °C and the 100% weight loss occurred in one step, suggesting the sublimation of these materials (Figure S9).<sup>29,30-31</sup> It has been previously suggested that the ammonium salts such as MABr are incorporated in the crystal lattice of the perovskite in the form of MA<sup>+</sup>/Br<sup>-</sup> and, as consequence, they can be released at a lower temperature than that of the ammonium salt.<sup>32</sup> The second step of the weight loss could be ascribed to the loss of ODE plus the remaining ammonium salts (plus OLA in the case of **P<sub>OA1</sub>**), while the third step is consistent with the loss of lead bromide of the perovskite. Interestingly, the sublimation temperature of the lead bromide in **P<sub>OA2</sub>** is more similar to that of PbBr<sub>2</sub> than to that of **P<sub>OA1</sub>**.

In addition, the solids obtained after the precipitation/centrifugation of **P<sub>OA1</sub>** and **P<sub>OA2</sub>** (Ss<sub>1</sub> and Ss<sub>2</sub>, respectively) were also studied by TGA. The spectra (Figure S12 and Figure S13) showed the presence of ca. 13% of the lead bromide. This could be ascribed to the non-complete precipitation of all the nanoparticles during the centrifugation step.

Further data on the composition of **P<sub>OA1</sub>** and **P<sub>OA2</sub>** samples were extracted by making use of their <sup>1</sup>H-NMR spectra, which gave information on the molar ratio of the organic components, combined with their TGA spectra, which gave information on the PbBr<sub>2</sub> weight percentage in the isolated mass. Figure S14-S17 showed the <sup>1</sup>H-NMR spectra of the pure precursors used in the

quantification.

The <sup>1</sup>H-NMR spectra of the supernatants were also analysed (spectra not included); the data obtained from them combined with those of the corresponding samples (**P<sub>OA1</sub>** and **P<sub>OA2</sub>** spectra in Figure S14 and Figure 5, respectively; spectra of the precursors are included in Figures S15-S18) were consistent with the amount of material used in the preparation of the nanoparticles. The molar composition of **P<sub>OA1</sub>** and **P<sub>OA2</sub>** as well as the yield of isolated perovskite are shown in Tables S3 and S4. These data indicated that the perovskite nanoparticles capped by the ammonium salts and ODE, which was incorporated into the organic capping via chain interdigitation between the alkyl chains, cooperated in their stability/dispersability.

It has been suggested that iodopentafluorobenzene passivates the excess of iodide ions on the surface of mixed halide (I, Cl) lead perovskites.<sup>33</sup> Therefore, we propose that the ammonium moiety of OA binds to the under-coordinated bromide ions of the perovskite nanoparticles.

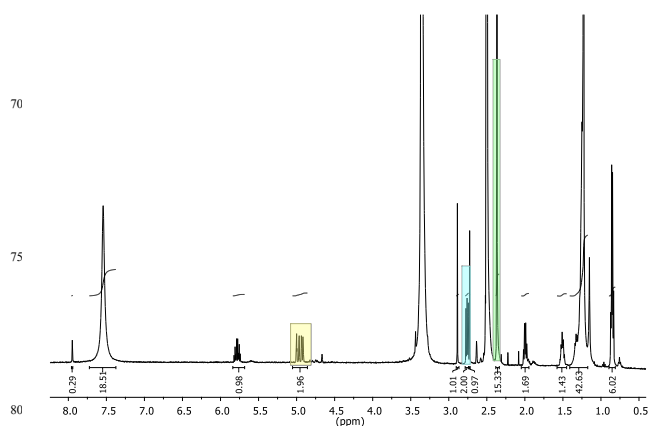


**Fig.5:** <sup>1</sup>H-NMR of **P<sub>OA2</sub>** in deuterated DMSO; the signal of MABr, OABr, and ODE used for the quantification are in green, cyan, and yellow, respectively.

In addition, ODE may bind to under-coordinated lead ions on the perovskite crystal surface via its double bond, thus passivating these defect sites and decreasing the rate of nonradiative recombination in the perovskite. It has recently been reported that weak Lewis bases can play a relevant role in the emissive properties of perovskites. Thus, Snaith *et al.* have recently suggested that thiophene and pyridine can bind to under-coordinated Pb atoms of mixed halide (Cl, I) lead perovskite films, thus enhancing their photoluminescence and solar cell performance (up to 16.5%).<sup>34-35</sup>

### 3.3 Time resolved photoluminescence analysis

Time-resolved photoluminescence spectroscopy was used to study the recombination lifetime of the **P<sub>OA1</sub>** and **P<sub>OA2</sub>** perovskites (in both the colloidal solution and the film). The PL decays were registered at  $\lambda_{em}$  ca. 520 nm, under both nitrogen and air atmosphere, and they were fitted with a triexponential function of time ( $t$ ),

$$I(t) = \sum_i \alpha_i \left(-\frac{t}{\tau_i}\right) \quad (1)$$

where  $\tau_i$  are the decay times and  $\alpha_i$  represents the amplitudes of the components. The emission lifetimes and their corresponding contributions to the total signal are shown in Table S5-S6. The average recombination lifetimes ( $\tau_{av}$ ) were estimated with the  $\tau_i$

and  $\alpha_i$  values from the fitted curve data according to equation 2.

$$\tau(av) = \frac{\sum \alpha_i \tau_i^2}{\sum \alpha_i \tau_i} \quad (2)$$

The  $\tau_{av}$  for  $\text{P}_{\text{OA1}}$  and  $\text{P}_{\text{OA2}}$  showed a slight dependence on the excitation wavelength (340, 405, 470 nm) and on the presence of oxygen (Table 1). Toluene colloidal solutions of  $\text{P}_{\text{OA2}}$  exhibited a considerably longer  $\tau_{av}$  than  $\text{P}_{\text{OA1}}$ , reaching values close to 600 ns in solution and ca. 410 ns in film. The last value is close to that recently reported for a  $\text{MAPbBr}_{3-x}\text{Cl}_x$  film. The radiative rate constant ( $k_r$ ) and the non-radiative rate constant ( $k_{nr}$ ) were estimated by using equations 3 and 4; where  $\Phi_{PL}$  is the photoluminescence quantum yield.

Average lifetime ( $\tau_{av}$ ), quantum yield ( $\Phi_{PL}$ ), radiative ( $k_r$ ) and non-radiative ( $k_{nr}$ ) constants;  $\lambda_{exc}=340$  nm.

$$\Phi_{PL} = k_r \cdot \tau_{av} \quad (3)$$

$$\tau_{av} = \frac{1}{(k_r + k_{nr})} \quad (4)$$

These data revealed the remarkably low value of  $k_{nr}$ , which was not only of the same order of magnitude as  $k_r$  but, except for the  $\text{P}_{\text{OA1}}$  film, was even five times lower. This evidenced the considerable reduction of surface defects that otherwise would trap excited electrons and decrease the emissive properties of the perovskites.

**Table 1**-Photoluminescence data of  $\text{P}_{\text{OA1}}$  and  $\text{P}_{\text{OA2}}$ .<sup>a</sup>

Sample	$\tau_{av}$ (ns)	$\Phi_{PL}$	$k_r$ ( $\text{s}^{-1}$ )	$k_{nr}$ ( $\text{s}^{-1}$ )
$\text{P}_{\text{OA1}}$ (air)	415.09	0.673	$1.61 \times 10^6$	$0.79 \times 10^6$
$\text{P}_{\text{OA1}}$ ( $\text{N}_2$ )	411.17	0.673	$1.64 \times 10^6$	$0.80 \times 10^6$
$\text{P}_{\text{OA1}}$ film	344.38	0.342	$0.99 \times 10^6$	$1.91 \times 10^6$
$\text{P}_{\text{OA2}}$ (air)	594.45	0.831	$1.39 \times 10^6$	$0.29 \times 10^6$
$\text{P}_{\text{OA2}}$ ( $\text{N}_2$ )	552.56	0.802	$1.45 \times 10^6$	$0.36 \times 10^6$
$\text{P}_{\text{OA2}}$ film	412.09	0.723	$1.75 \times 10^6$	$0.67 \times 10^6$

<sup>a</sup> Excitation at 340 nm.

### 3.4 Stability and photostability of $\text{P}_{\text{OA1}}$ and $\text{P}_{\text{OA2}}$ samples

$\text{P}_{\text{OA2}}$  stored as solid in the dark and under air atmosphere preserved their emissive properties for more than five months while and  $\text{P}_{\text{OA1}}$  was considerably less stable.

The photostability of  $\text{P}_{\text{OA1}}$  and  $\text{P}_{\text{OA2}}$  colloidal solutions under light irradiation in the presence and in the absence of air was studied under two different light sources: fluorimeter lamps ( $\lambda_{exc}$  at 350 nm) and visible lamps (8 lamps, 400-700 nm, maximum centred at 420 nm). UV irradiation of  $\text{P}_{\text{OA2}}$  under air atmosphere led to a loss of 7% emission intensity in the first 30 min and an additional loss of 10% after the following 481 min (Figure 6). Also  $\text{P}_{\text{OA1}}$  presented high photostability with <10% decrease of luminescence after 183 min of excitation at 350 nm (Figure not shown). Finally,  $\text{P}_{\text{OA2}}$  photoluminescence decreased only a 6% after visible-light irradiation 75 min under air atmosphere (Figure S19).

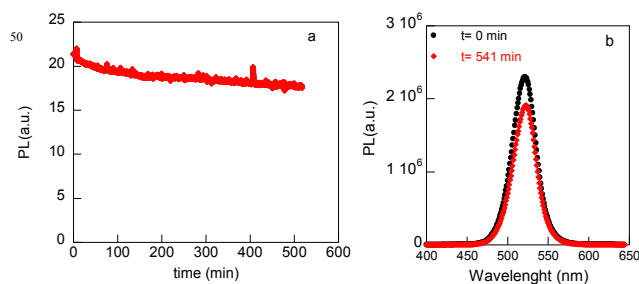


**Fig. 6:** (a) Photoluminescence of  $\text{P}_{\text{OA2}}$  dispersed in toluene as a function of the irradiation time:  $\lambda_{exc}=350$ , PL registered at 520 nm under air atmosphere. (b) Photoluminescence spectra before and after 541 minutes of irradiation.

## Conclusions

We have demonstrated here that highly luminescent and photostable  $\text{CH}_3\text{NH}_3\text{PbBr}_3$  nanoparticles can be prepared by following the strategies described for the synthesis of other materials confined in the three dimensions (i.e., zero-dimension material). Completion of the coordination sphere of the ions at the nanoparticle surface may be the origin of the low non-radiative recombination rate constant of these nanoparticles. While the ammonium cation may bind to the under-coordinated bromide anions, a weak Lewis base, such as 1-octadecene, may bind to the under-coordinated Pb cations. The fine-tuning of the molar ratio of all the components eventually provides nanoparticles with a high photoluminescence recombination lifetime (>420 ns) and photostability under UV light (<18% emission loss after 8.5 h). This perovskite preserves its emissive properties in the solid state, which makes it promising for light emitting devices and photovoltaic applications.

## Acknowledgment

We thank MINECO (Project CTQ2011-27758, contract granted to S.G-C), GVA (ACOMP/2013/008) and FGUV (R.E.G contract).

## Notes and references

<sup>a</sup> Instituto de Ciencia Molecular (ICMol), Universidad de Valencia, Catedrático José Beltrán 2, 46980, Paterna, Valencia, Spain. Fax: 34963543273; Tel: 34963544307; E-mail: Raquel.galian@uv.es, julia.perez@uv.es

† Electronic Supplementary Information (ESI) available: additional absorption, emission, TGA, XPS, NMR spectra for perovskite and precursors and tables with photophysical and nanoparticle composition data. See DOI: 10.1039/b000000x/

1. D. B. Mitzi, in *Progress in Inorganic Chemistry*, John Wiley & Sons, Inc., 2007, pp. 1-121.
2. C. S. Ponseca, T. J. Savenije, M. Abdellah, K. Zheng, A. Yartsev, T. Pascher, T. Harlang, P. Chabera, T. Pullerits, A. Stepanov, J.-P. Wolf and V. Sundström, *Journal of the American Chemical Society*, 2014, **136**, 5189-5192.
3. O. D. Miller, E. Yablonovitch and S. R. Kurtz, *Photovoltaics, IEEE Journal of*, 2012, **2**, 303-311.
4. F. Deschler, M. Price, S. Pathak, L. E. Klintberg, D.-D. Jarausch, R. Higler, S. Hüttner, T. Leijtens, S. D. Stranks, H. J. Snaith, M.

- Atatüre, R. T. Phillips and R. H. Friend, *The Journal of Physical Chemistry Letters*, 2014, **5**, 1421-1426.
- 5 N.-G. Park, *Materials Today*, 2014, DOI: **10.1016/j.mattod.2014.07.007**.
- 5 6 L. Etgar, P. Gao, Z. Xue, Q. Peng, A. K. Chandiran, B. Liu, M. K. Nazeeruddin and M. Grätzel, *Journal of the American Chemical Society*, 2012, **134**, 17396-17399.
- 7 M. M. Lee, J. Teuscher, T. Miyasaka, T. N. Murakami and H. J. Snaith, *Science*, 2012, **338**, 643-647.
- 10 8 H.-S. Kim, C.-R. Lee, J.-H. Im, K.-B. Lee, T. Moehl, A. Marchioro, S.-J. Moon, R. Humphry-Baker, J.-H. Yum, J. E. Moser, M. Grätzel and N.-G. Park, *Sci. Rep.*, 2012, **2**.
- 9 A. Kojima, M. Ikegami, K. Teshima and T. Miyasaka, *Chemistry Letters*, 2012, **41**, 397-399.
- 15 10 S. D. Stranks, G. E. Eperon, G. Grancini, C. Menelaou, M. J. P. Alcocer, T. Leijtens, L. M. Herz, A. Petrozza and H. J. Snaith, *Science*, 2013, **342**, 341-344.
- 11 D. V. Talapin, A. L. Rogach, E. V. Shevchenko, A. Kornowski, M. Haase and H. Weller, *Journal of the American Chemical Society*, 2002, **124**, 5782-5790.
- 20 12 C. Wehrenfennig, G. E. Eperon, M. B. Johnston, H. J. Snaith and L. M. Herz, *Advanced Materials*, 2014, **26**, 1584-1589.
- 13 J. H. Noh, S. H. Im, J. H. Heo, T. N. Mandal and S. I. Seok, *Nano Letters*, 2013, **13**, 1764-1769.
- 25 14 M. Zhang, H. Yu, M. Lyu, Q. Wang, J.-H. Yun and L. Wang, *Chemical Communications*, 2014, **50**, 11727-11730.
- 15 S. Ryu, J. H. Noh, N. J. Jeon, Y. Chan Kim, W. S. Yang, J. Seo and S. I. Seok, *Energy & Environmental Science*, 2014, **7**, 2614-2618.
- 30 16 E. Edri, S. Kirmayer, M. Kulbak, G. Hodes and D. Cahen, *The Journal of Physical Chemistry Letters*, 2014, **5**, 429-433.
- 17 L. C. Schmidt, A. Pertegás, S. González-Carrero, O. Malinkiewicz, S. Agouram, G. Mínguez Espallargas, H. J. Bolink, R. E. Galian and J. Pérez-Prieto, *Journal of the American Chemical Society*, 2014, **136**, 850-853.
- 35 18 J. Aguilera-Sigalat, S. Rocton, J. F. Sanchez-Royo, R. E. Galian and J. Perez-Prieto, *RSC Advances*, 2012, **2**, 1632-1638.
- 19 J. Pérez-Prieto, *Photochemistry and Photobiology*, 2013, **89**, 1291-1298.
- 40 20 O. Knop, R. E. Wasylshen, M. A. White, T. S. Cameron and M. J. M. V. Oort, *Canadian Journal of Chemistry*, 1990, **68**, 412-422.
- 21 A. Poglitsch and D. Weber, *The Journal of Chemical Physics*, 1987, **87**, 6373-6378.
- 45 22 W. E. Morgan and J. R. Van Wazer, *The Journal of Physical Chemistry*, 1973, **77**, 964-969.
- 23 R. Lindblad, D. Bi, B.-w. Park, J. Oscarsson, M. Gorgoi, H. Siegbahn, M. Odelius, E. M. J. Johansson and H. Rensmo, *The Journal of Physical Chemistry Letters*, 2014, **5**, 648-653.
- 50 24 S. Chen, T. W. Goh, D. Sabba, J. Chua, N. Mathews, C. H. A. Huan and T. C. Sum, *APL Materials*, 2014, **2**, -.
- 25 R. E. Galian, M. de la Guardia and J. Pérez-Prieto, *Langmuir*, 2011, **27**, 1942-1945.
- 26 A. Adenier, M. M. Chehimi, I. Gallardo, J. Pinson and N. Vilà, *Langmuir*, 2004, **20**, 8243-8253.
- 55 27 H. Kanai, M. Yoshiki, M. Hayashi, R. Kuwae and Y. Yamashita, *Journal of the American Ceramic Society*, 1994, **77**, 2229-2231.
- 28 C. A. Cattley, A. Stavrinadis, R. Beal, J. Moghal, A. G. Cook, P. S. Grant, J. M. Smith, H. Assender and A. A. R. Watt, *Chemical Communications*, 2010, **46**, 2802-2804.
- 29 These results contrast with the theoretical prediction that primary ammonium bromides decompose to the corresponding amine plus HBr. Ref.30
- 60 30 A. Dualeh, P. Gao, S. I. Seok, M. K. Nazeeruddin and M. Grätzel, *Chemistry of Materials*, 2014.
- 31 M. Sawicka, P. Storonik, P. Skurski, J. Błażejowski and J. Rak, *Chemical Physics*, 2006, **324**, 425-437.
- 32 Y. Zhao and K. Zhu, *Journal of the American Chemical Society*, 2014, **136**, 12241-12244.
- 70 33 A. Abate, M. Saliba, D. J. Hollman, S. D. Stranks, K. Wojciechowski, R. Avolio, G. Grancini, A. Petrozza and H. J. Snaith, *Nano Letters*, 2014, **14**, 3247-3254.
- 34 N. K. Noel, A. Abate, S. D. Stranks, E. S. Parrott, V. M. Burlakov, A. Goriely and H. J. Snaith, *ACS Nano*, 2014, **8**, 9815-9821.
- 75 35 I. A. Shkrob and T. W. Marin, *The Journal of Physical Chemistry Letters*, 2014, **5**, 1066-1071.
- 80



Highly luminescent and photostable  $\text{CH}_3\text{NH}_3\text{PbBr}_3$  nanoparticles have been prepared by fine-tuning the molar ratio between  $\text{CH}_3\text{NH}_3\text{Br}$ ,  $\text{PbBr}_2$ , a medium-size alkyl-chain ammonium salt, and 1-octadecene.

